Development of Timber Buckling Restrained Brace for Mass Timber-Braced Frames

Colton Murphy[1]; Chris P. Pantelides, M.ASCE[2]; Hans-Erik Blomgren, M.ASCE[3]; and Douglas Rammer, M.ASCE[4]

Abstract: This research presents the development of a mass timber buckling restrained brace (T-BRB) that combines a low yield strength steel core with a mass timber casing to create a new ductile fuse. The T-BRB is an essential element of a mass timber buckling restrained braced frame (BRBF), which is a promising mass timber wood lateral force–resisting system. Critical elements of T-BRB design that are important for good performance include casing stiffness, casing material, number and spacing of bolts, timber spacer and casing gap, steel core yield strength, and friction between steel core and casing interface. Compressive tests on engineered wood blocks using glued laminated timber, laminated veneer lumber, parallel strand lumber, and mass plywood panel (MPP) were conducted to determine elastic stiffness, maximum load, and ultimate displacement. MPP loaded parallel to the wide face of laminations (X-direction) outperformed other materials with respect to high elastic stiffness, which is an important property of the casing because it controls buckling of the steel core. Six 3.66 m (12 ft)–long T-BRBs with a targeted yield strength of 274 kN (61.5 kip) were tested utilizing three T-BRB casing designs with varying MPP lamination layups. A 3.9% strain was achieved under a strain-based loading protocol. For a fatigue-based loading protocol, after two cycles at 2.0% strain, more than 26 additional cycles at 1.5% strain were attained. The hysteresis curves for all six T-BRBs remained stable throughout the tests and the cumulative inelastic deformation exceeded two times the value required by the standard. **DOI: 10.1061/(ASCE)ST.1943-541X.0002996.**

Author keywords: Brace; Buckling; Buckling restrained braced frame; Building; Damping; Fuse; Mass timber; Structure.

Introduction

There is a growing movement to use mass timber as a primary structural material for medium-height and tall buildings, in large part because timber is renewable, it stores carbon, and it is energy efficient. In conventional braced timber frames under seismic loads, the connections between timber braces and the main frames are relied on to dissipate hysteretic energy; however, these connections can be severely damaged in strong earthquakes and limit system ductility. There are currently no approved mass timber lateral force–resisting systems in building codes recognized in the United States. Buckling restrained braced frames (BRBFs) are code approved, proven, and a reliable method for providing an efficient lateral force–resisting system for structural steel structures in earthquake-prone regions. Specifically, timber buckling restrained braces (T-BRBs) are capable of providing high load and deformation in both compression and tension unlike conventional timber braces. This research is key for creating a mass timber BRBF system for eventual building code adoption. The buckling restrained brace (BRB) is a fuse element that facilitates stable energy dissipation while being replaceable after an earthquake. Mass timber buildings can benefit from lightweight and aesthetic lateral force–resisting systems that provide the structural performance benefits of a BRBF.

Conventional composite steel/concrete BRBs provide stiffness, strength, and stable energy dissipation (Black et al. 2004); in addition, they provide adequate rigidity to satisfy allowable story drift. Lightweight and inexpensive fuse-type BRBs facilitate replaceability, ease of handling, and condition assessment after an earthquake (Tabatabaei et al. 2014). The design of composite steel/concrete BRB casing dimensions is based on principles for avoiding global buckling (Watanabe et al. 1988). Research aimed at exploring the high-mode buckling response of conventional BRB steel cores has improved our understanding of the internal modal response (Wu et al. 2014). Methods for design of the casing have been developed that can resist both weak-axis and strong-axis steel core buckling in conventional BRBs (Xu and Pantelides 2017). The bulging force from localized weak-axis core buckling can be predicted and prevented using adequate casing design (Lin et al. 2011). Large gaps between the core and casing diminish the ability of BRBs to dissipate energy in compression (Genna and Gelfi 2012); the gaps exacerbate lateral casing thrust and make internal forces difficult to predict; a gap allows premature steel core buckling and ultimately reduces hysteretic energy dissipation.

Advancements in timber technology are making midrise mass timber buildings attractive. Mass timber buildings attract lower inertial forces but they lack a code-defined lateral force–resisting system. Ductility, strength, stiffness, and damping of conventional timber braces is a concern in high seismic regions; care must be taken in the design of the connections to reach high displacement ductility (Popovski 2000).

S. E. Pryor, P. Flynn, and W. Downs ["Buckling restrained braced frame," US Patent 20050257490A1 (2005)] presented a

[1]Graduate Research Assistant, Dept. of Civil and Environmental Engineering, Univ. of Utah, Salt Lake City, UT 84112. Email: coltonfmurphy@gmail.com

[2]Professor, Dept. of Civil and Environmental Engineering, Univ. of Utah, Salt Lake City, UT 84112 (corresponding author). Email: c.pantelides@utah.edu

[3]Structural Engineer, Katerra, 542 1st Ave. S #4, Seattle, WA 98104. Email: hans-erik.blomgren@katerra.com

[4]Research Engineer, UDSA Forest Products Laboratory, One Gifford Pinchot Dr., Madison, WI 53726. Email: douglas.r.rammer@usda.gov

Note. This manuscript was submitted on March 10, 2020; approved on December 30, 2020; published online on February 27, 2021. Discussion period open until July 27, 2021; separate discussions must be submitted for individual papers. This paper is part of the ***Journal of Structural Engineering***, © ASCE, ISSN 0733-9445.

buckling restrained brace concept using a lightweight casing made of solid wood; however, the mechanism of a brace using engineered mass timber to restrain buckling of a rectangular steel core was not explored. A buckling restrained brace with a glued laminated timber (glulam) casing was built and tested under cyclic loads (Blomgren et al. 2016). The heavy timber buckling restrained brace (HT-BRB) exhibited higher axial load, higher stiffness, stable axial deformation capacity, and greater energy dissipation compared to conventional timber braces. A high elastic stiffness is desirable for a T-BRB casing; when the transverse modulus of elasticity of the timber casing is too low, failure due to compression perpendicular to grain leads to premature weak-axis core plate buckling.

Timber construction is sustainable and environmentally friendly (Zhang et al. 2018). Timber is an excellent building material because it is renewable with good strength-to-weight ratio and good insulating properties, and it acts as a carbon sink (Cuadrado et al. 2015). To advance taller timber structures such as the 18-story Mjøstårnet mass timber building (Abrahamsen 2017) to be used in seismic regions, an efficient lateral force–resisting system is needed.

A ductile lateral force–resisting system is proposed for mass timber buildings in seismic regions. This paper extends recent work performed in the development of a timber BRB seeking an efficient lateral force–resisting system for mass timber buildings (Blomgren et al. 2016; Murphy et al. 2019; Murphy 2020). The purpose of this research is to validate the mass timber casing as a buckling restraining mechanism and evaluate the seismic performance of the T-BRB design. In particular, the casing of the T-BRB must have the right balance of strength and stiffness. Previous research by Blomgren et al. (2016) demonstrated detrimental short-wave buckling failures in the glulam casing perpendicular to grain because there was insufficient strength or stiffness.

The present investigation performs an assessment of alternate materials, casing design, steel element behavior, and evaluation of the cyclic performance of the T-BRB. To determine a viable engineered timber casing for T-BRBs, blocks of various timber materials were tested in compression to determine mechanical properties for the casing. Specific timber materials, and direction of load either parallel or perpendicular to the wide face of the lamination were considered as variables.

The research aims to provide a summary of the methods used to proportion the T-BRB specimens, explain the physics and mechanics of how the elements of the T-BRB function and describe the overall hysteretic performance of the T-BRB. The objective of this research was to develop a mass timber BRB that is easy and economical to construct and feasible to implement by combining a low yield strength steel core with a mass timber casing for use in buckling restrained braced frames. To be successful, the T-BRB must satisfy the cumulative inelastic deformation requirements of AISC 341 (AISC 2016).

Experimental Evaluation of T-BRB Timber Casing

A key concept of T-BRB design is finding a wood material to act as the casing with low variability in its properties that allows the steel core to locally buckle without premature splitting under cyclic loading. Various engineered timber materials were tested to determine the most suitable timber casing for the design of a T-BRB. Screws were examined as a means to improve premature splitting of glulam and parallel-strand lumber (PSL) materials. Information on test results with screw reinforcement is not included here because screws were not used to construct the T-BRBs; the interested reader can access this information elsewhere (Murphy et al. 2019; Murphy 2020).

Timber Casing Materials

The compressive strength of engineered wood such as laminated veneer lumber (LVL), PSL, glulam, and mass plywood panel (MPP) was investigated for possible use as the timber casing of T-BRB. The Douglas fir LVL and Douglas fir PSL specimens were sourced from material qualified by ASTM D5456 (ASTM 2019b) requirements. PSL is a wood composite with stranded wood fibers primarily oriented along the longitudinal axis of the member. Glulam specimens were generated from the inner plies (Grade D) of a Douglas fir beam manufactured to CSA O122-16 (CSA 2016). At the time of testing, the MPP panels were in the product development stage, and have subsequently been qualified under the APA PR-L325 (APA 2019) standard as a cross-laminated timber product with 25.4-mm (1.0-in.) structural composite lumber (SCL) laminations.

Compression Tests for Various Timber Casing Materials

Fig. 1 shows the test setup for compression tests of timber casing materials. All blocks were 152 × 152 × 305 mm (6 × 6 × 12 in.). A 76 × 76 mm (3 × 3 in.) steel fixed head platen was used to apply vertical compression. Two test repetitions were carried out for each timber material. Both monotonic and cyclic tests were carried out. The cyclic tests followed ASTM E2126 Method C (ASTM 2011) with a loading rate of 1.0 Hz. Glulam and MPP were loaded parallel (*X*-direction) and perpendicular (*Y*-direction) to the wide face of laminations according to ASTM D5456 (ASTM 2019). LVL was loaded in the *X*- and *Y*-directions according to ASTM D5456 (ASTM 2019) convention. PSL was loaded only in the *X*-direction.

The deformation and failure mode of the blocks after testing are shown in Fig. 2. Fig. 2(a) shows a glulam block loaded in the *X*-direction, Fig. 2(b) shows an LVL bloc, Fig. 2(c) shows a PSL block, and Fig. 2(d) shows an MPP block. The entire series of compression test results can be found elsewhere (Murphy et al. 2019; Murphy 2020).

A selected sample of the load versus displacement graphs from the monotonic compression tests is shown in Fig. 3. The nomenclature used is as follows: M = MPP, G = glulam, P = PSL, L = LVL; X = parallel to the wide face of the lamination for G, M, and L

Fig. 1. Compression test setup for LVL block loaded in the *X*-direction. [Orientation according to ASTM D5456 (ASTM 2019).]

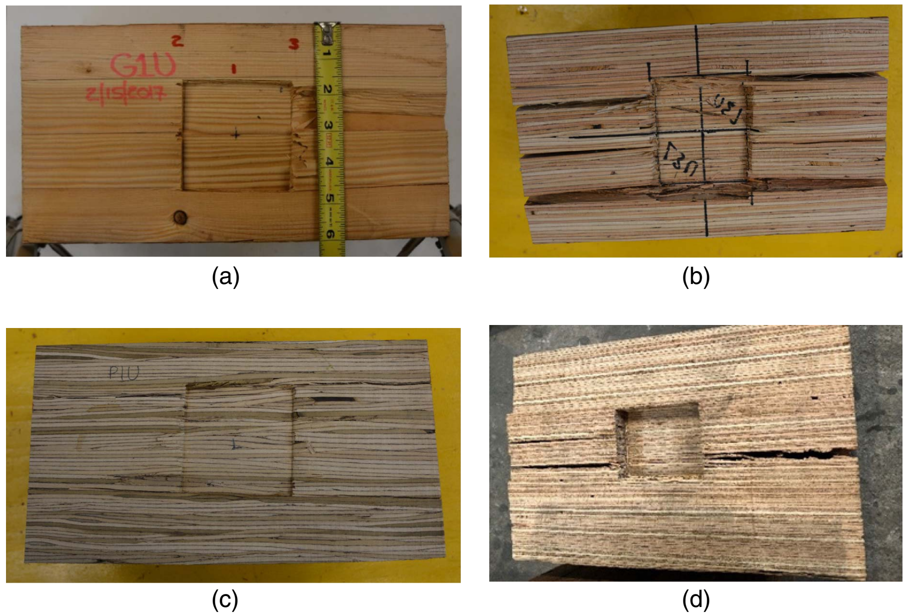

Fig. 2. Deformation of blocks after compression load test: (a) glulam; (b) LVL; (c) PSL; and (d) MPP.

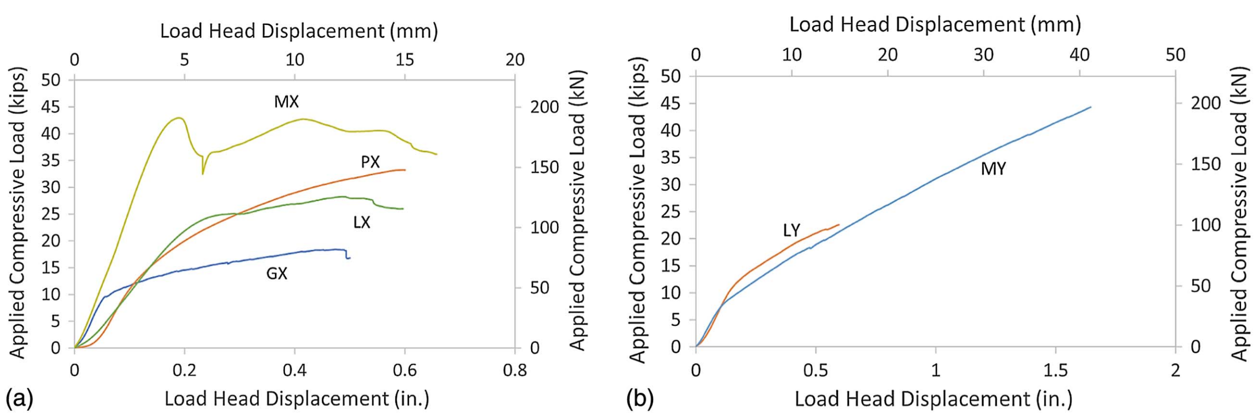

Fig. 3. Monotonic compression block results: (a) loaded in X-direction; and (b) loaded in Y-direction.

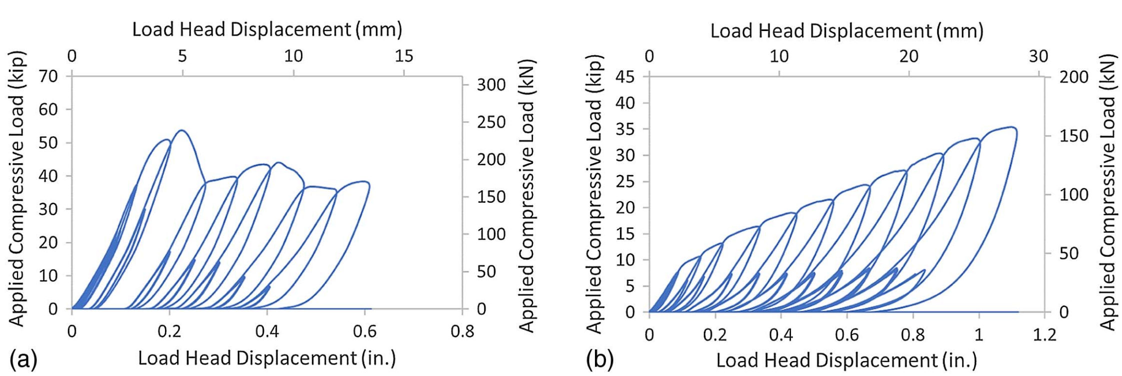

Fig. 4. Cyclic compression hysteresis curves for typical MPP material: (a) loaded in X-direction; and (b) loaded in Y-direction.

and all PSL blocks, and Y = perpendicular to the wide face of the lamination. Fig. 3(a) shows results for blocks loaded monotonically in the X-direction. Fig. 3(b) shows blocks loaded monotonically in the Y-direction. Compression stiffness was determined by linear regression over the data between 20% and 40% of the maximum load. Improved stiffness and maximum load were observed when compression was applied in the X-direction for the MPP material.

Fig. 4 shows hysteresis results for a typical MPP material. The cyclic tests show that MPP loaded in the Y-direction has a lower yield force when compared to the X-direction; MPP has a

Table 1. Test results for blocks under cyclic loading protocol

Material, orientation	P_{max} [kN (kip)]	Δ_{max} [mm (in.)]	Stiffness [kN/m (kip/in.)]
Glulam, *X*	113 (25.4)	20 (0.8)	20,825 (119)
PSL, *X*	184 (41.4)	23 (0.9)	21,350 (122)
LVL, *X*	142 (31.9)	13 (0.5)	23,625 (135)
MPP, *Y*	160 (36.0)	30 (1.2)	16,450 (94)
MPP, *X*	225 (50.5)	15 (0.6)	44,625 (255)

Note: Orientation according to ASTM D5456 (ASTM 2019).

hardening characteristic and performs in a more ductile manner. MPP loaded in the *Y*-direction underperforms MPP loaded in the *X*-direction based on the initial stiffness and strength. Table 1 summarizes the test results for blocks under cyclic compression load. Glulam underperforms when compared to other engineered wood materials and fails before reaching a 2.5-mm (0.1-in.) deformation. MPP was selected as the BRB casing material due to its superior strength and stiffness characteristics.

Compression Tests for Three MPP Casing Materials

While MPP was chosen as the best casing of the engineered timber materials tested, additional tests on certified MPP with new and different lamination layups were needed. MPP is an orthogonally composite material with different characteristics depending on the direction of applied force. The MPP casing layup utilized 25.4 mm (1.0 in.) Douglas fir laminations of varying elastic moduli equal to either 6,895 MPa (1.0×10^3 ksi) or 11,031 MPa (1.6×10^3 ksi). The modulus of elasticity per 25.4-mm (1.0-in.) layer is adjusted based on the ratio of long-ply to cross-ply veneers. The higher-modulus layers have more long-ply laminations than cross-ply laminations. Each 25.4-mm (1.0-in.) LVL lamination is composed of nine 3.2-mm (1/8-in.) veneers. The orientation of the wood grain in the nine layers adjusts the modulus of elasticity per 25.4-mm (1.0-in.) lamination. The three MPP layups were classified as 60/40, 80/20, and 100/0, which pertains to the percentage of 11,031 MPa (1.6×10^3 ksi) laminations to 6,895 MPa (1.0×10^3 ksi) laminations, as shown in Fig. 5. The 60/40 casing consisted of four center 25.4 mm (1.0 in.)–thick laminations of

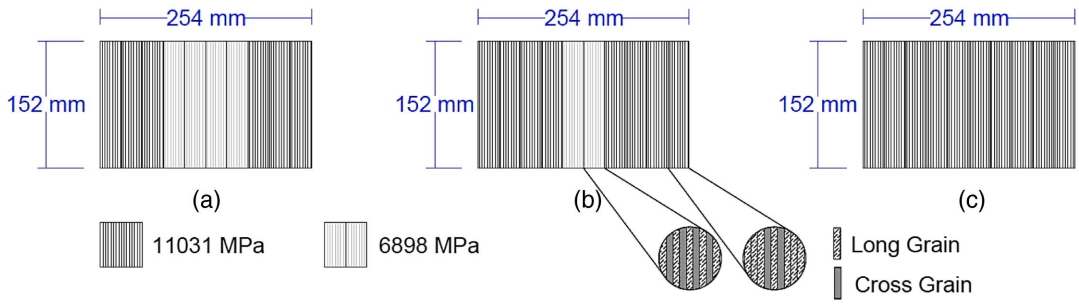

Fig. 5. MPP layout for three casing layups: (a) 60/40; (b) 80/20; and (c) 100/0.

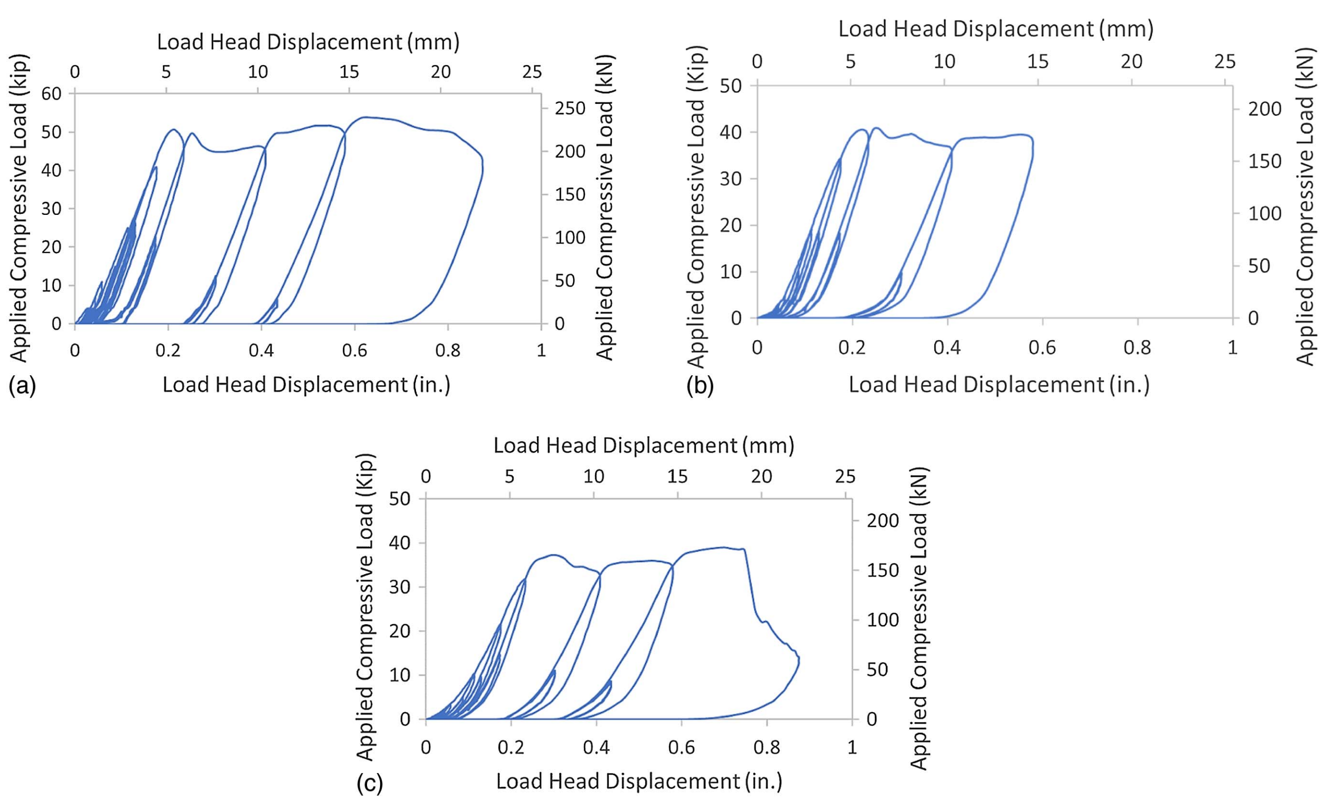

Fig. 6. Cyclic compression hysteresis from MPP block tests loaded in *X*-direction: (a) 60/40; (b) 80/20; and (c) 100/0.

Table 2. Lamination ply direction, average of maximum compressive load, maximum displacement, and elastic stiffness for three MPP layups

MPP layups	No. of long-ply laminations	No. of cross-ply laminations	P_{max} [kN (kip)]	Δ_{max} [mm (in.)]	Stiffness [kN/m (kip/in.)]
MPP-60/40	62	28	230 (51.6)	20 (0.8)	49,875 (285)
MPP-80/20	66	24	200 (44.9)	15 (0.6)	46,725 (267)
MPP-100/0	70	20	161 (36.2)	23 (0.9)	39,725 (227)

6,895 MPa (1.0×10^3 ksi) SCL with three outer laminations on each side of 11,031 MPa (1.6×10^3 ksi) SCL as shown in Fig. 5(a). The 80/20 casing contained only two 25.4 mm (1.0 in.)–wide laminations of 6,895 MPa (1.0×10^3 ksi) SCL, with the remaining laminations made of 11,031 MPa (1.6×10^3 ksi) SCL as shown in Fig. 5(b). The 100/0 casing was entirely made of 11,031 MPa (1.6×10^3 ksi) SCL, as shown in Fig. 5(c).

Fifteen compression tests were conducted to characterize the three specific MPP casing materials selected to study variations in MPP laminate construction. The same loading protocols were used to determine stiffness, maximum compression, and hysteresis curves. All samples were loaded in the X-direction; three hysteresis curves of MPP blocks are shown in Fig. 6. The average maximum compression, maximum displacement, and elastic stiffness for the three MPP layups are listed in Table 2. The MPP layup with the lowest specified modulus of elasticity (60/40) provides a higher localized stiffness when loaded in the X-direction because of the larger number of cross-ply laminations (28) aligned in the direction of the applied load.

Design of T-BRB

The material and dimensions of the timber casing must have the right balance of strength and stiffness to create a successful T-BRB. The design of the steel core, timber casing, and bolts must be validated by full-scale tests. Six 3.66 m (12 ft)–long T-BRBs with a design yield strength of 274 kN (61.5 kip) were tested. Three T-BRBs were tested using a fatigue protocol in which a high number of cycles was applied at a 1.5% strain, after two cycles at 2.0% strain were applied. The remaining three T-BRBs were tested using a strain loading protocol in which two cycles per strain level were applied at increasing displacement until failure.

T-BRB Specimen Layout

Steel Core Layout

The six T-BRBs were constructed using a 283-MPa (41-ksi) ASTM A36 (ASTM 2019a) steel core and an MPP casing as shown in Fig. 7. The design value for yield stress was taken as 283 MPa (41 ksi) and the tensile strength was taken as 431 MPa (62.5 ksi) from steel coupon tensile tests; a low yield strength steel core was selected to improve ductility and cyclic performance. The steel core cross section of the 2.49 m (98 in.)–long yielding length was 76 mm (3.0 in.) wide and 12.7 mm (0.5 in.) thick. Stiffener plates were fabricated from the same material as the steel core; they were welded to the steel core to prevent buckling outside the timber casing. Two cheek plates were welded to the ends of the T-BRBs around the pin connection to prevent tear-out failure. A 76×25 mm (3×1 in.) steel

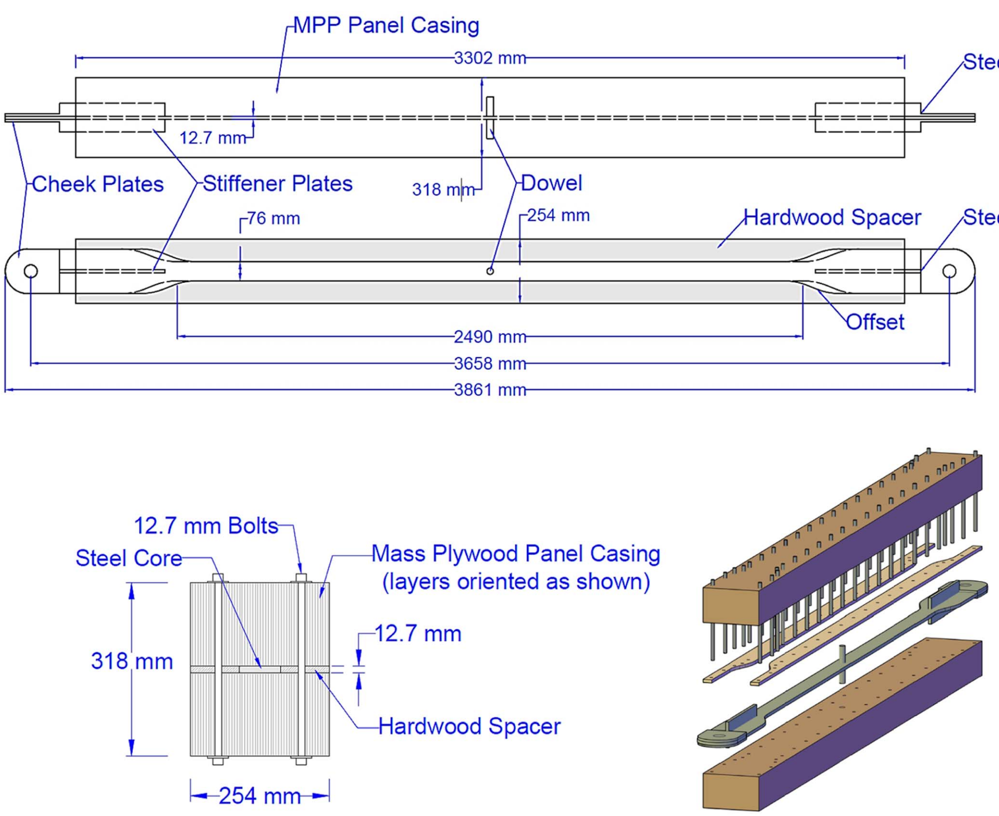

Fig. 7. T-BRB layout and three-dimensional visualization.

dowel was welded to the midlength of the steel core on both sides to ensure the casing remained centered throughout testing to encourage an even distribution of core buckling forces.

Hardwood Spacer Layout

A hardwood spacer was used to prevent strong-axis buckling of the steel core; the hardwood spacer transfers the forces arising from strong-axis buckling of the steel core to the bolts and ultimately to the MPP laminations. A laminated beechwood material was used for the spacer. The material was cut to the profile necessary to fill the void made by the steel core between the timber casing, as shown in Fig. 7. Offsets were included to allow for movement of the steel core when placed under compression.

MPP Casing Layout

Fig. 7 is a three-dimensional view of the T-BRB showing the MPP casing, the bolts, the steel core, and the hardwood spacer. The three MPP casing layups described in Fig. 5 were used to build the six T-BRBs. The MPP casing was composed of two pieces that were 254 mm (10 in.) wide and 152 mm (6 in.) thick. T-BRB Specimens

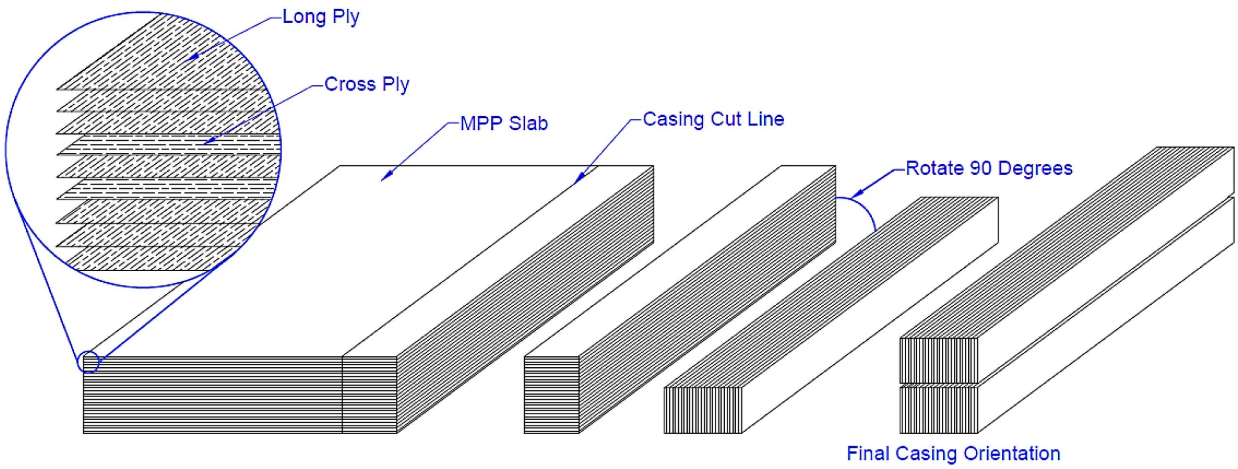

Fig. 8. MPP slab cut and casing orientation with 11,031-MPa (1,600-ksi) lamination magnification.

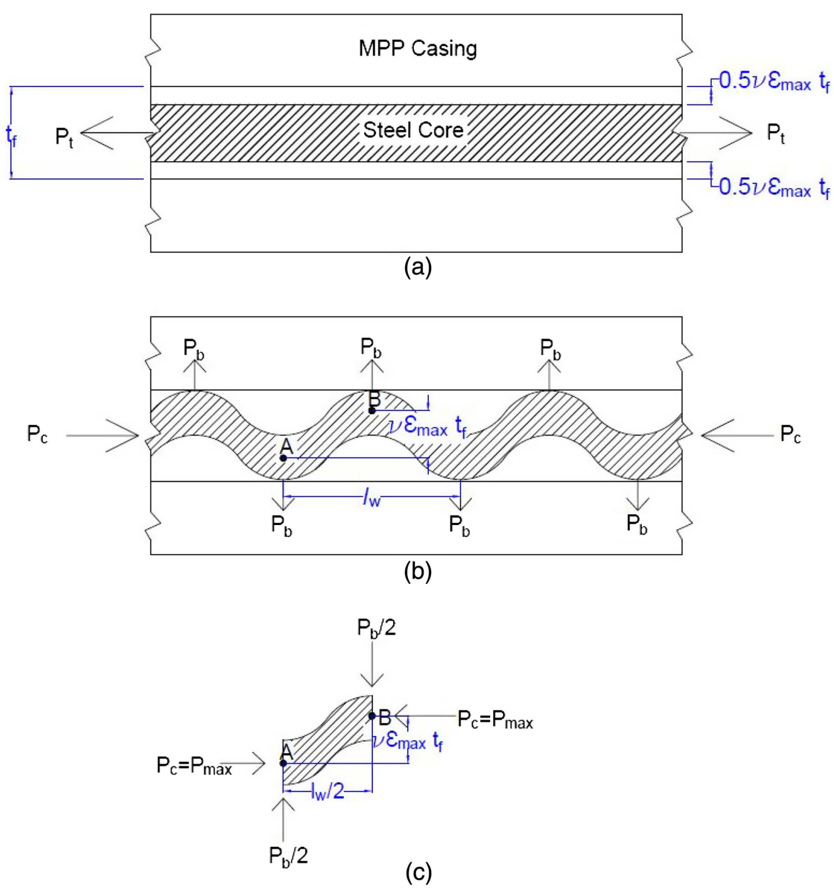

Fig. 9. Mechanics of buckling: (a) tensile load; (b) compressive load; and (c) free-body diagram.

1–3 used 60/40, 80/20, and 100/0 casing, respectively; T-BRB Specimens 4–6 used 100/0, 80/20, and 60/40 casing, respectively. Fig. 8 shows the MPP panel slab and timber casing layout. The sequence of building the timber casing from the two 254 mm (10 in.)–wide and 152 mm (6 in.)–thick pieces is important. The MPP layup with the lowest specified modulus of elasticity (60/40) provides a higher localized stiffness when loaded in the *X*-direction because of the larger number of cross-ply laminations (28) that are aligned in the direction of the applied load and thus has the largest stiffness when rotated 90°, as shown in Fig. 8.

T-BRB Design Elements

Timber Casing Design

The timber casing prevents global buckling of the T-BRB. Weak-axis buckling of the core typically controls design of the casing. The timber casing was designed following the guidelines for a steel casing (Watanabe et al. 1988); Euler buckling load of the casing should be 1.5 times larger than the yield load of the steel core to account for material overstrength, strain hardening, and friction forces. The design yield strength of the steel core was 283 MPa (41 ksi) and the cross-sectional area was 968 mm^2 (1.5 $in.^2$), resulting in a yield force of 274 kN (61.5 kip). The Euler buckling strength of the casing was sized to resist 1.5 times the yield strength of the core, or 410 kN (92.3 kip).

The end conditions of the T-BRB were assumed pinned; therefore, n is equal to 1.0. The length of the casing was 3.30 m (130.0 in.). The two casing pieces act compositely once they are bolted together. The modulus of elasticity, E, was determined using the APA product report (APA 2020). The fifth percentile modulus in the minor strength direction of the material was used (Zahn and Rammer 1995; Rammer and Zahn 1997); this value was obtained as 1,365 MPa (198 ksi). The Euler buckling load of the casing is found using Eq. (1)

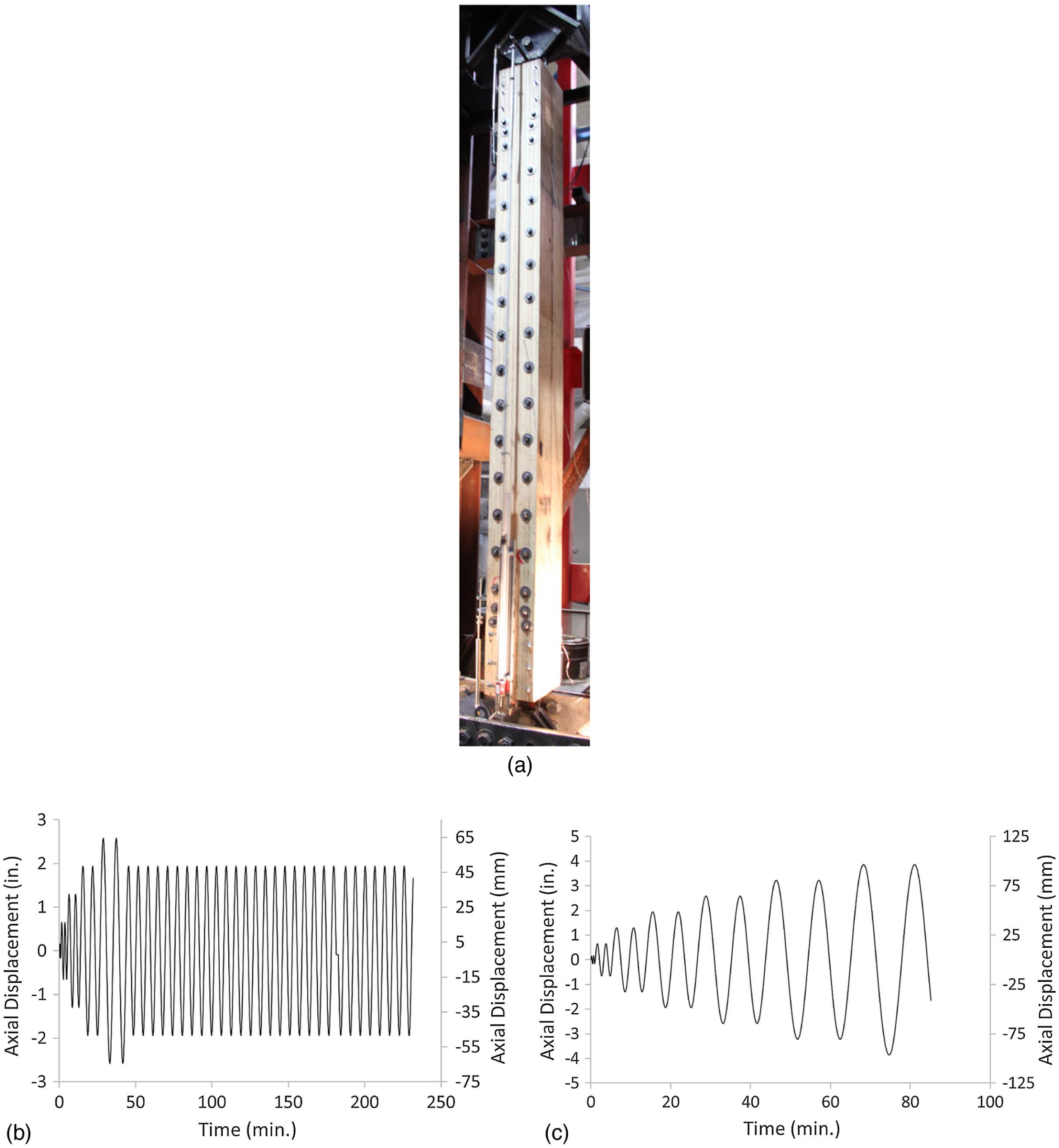

Fig. 10. T-BRB test setup and loading protocols: (a) T-BRB test setup; (b) fatigue protocol for Specimens 1–3; and (c) strain protocol for Specimens 4–6.

$$P_E = \frac{n\pi^2(EI)}{L^2} \tag{1}$$

Solving for the unknown moment of inertia, I, the required dimensions of the casing were found as 254 mm (10.0 in.) by 267 mm (10.5 in.). The 254-mm (10.0-in.) dimension is fixed due to the maximum available thickness of the MPP panel. The final dimensions of the casing were conservatively selected as 254 mm (10.0 in.) by 318 mm (12.5 in.), which includes the hardwood spacer.

Bolt Design

Two rows of 12.7-mm (1/2-in.) diameter, A449 bolts with 81-kN (18.4-kip) yield capacity were used to connect the two sides of the MPP casing including the hardwood spacer; the tensile yield strain of the bolts is 3,200 microstrain. A 50.8-mm (2.0-in.) edge distance and a 178-mm (7.0-in.) bolt spacing were used along the yielding length of the T-BRB; this spacing was reduced near the ends to account for an increase in out-of-plane forces. When the steel is in tension, a gap forms between the steel core and timber casing of increasing amplitude throughout the cyclic test due to Poisson effects. To minimize this gap, the T-BRB was constructed without any initial gap between the steel core and timber casing. Using Fig. 9(a) as the free-body diagram of the buckled core inside the casing results in a gap equal to

$$\Delta_{\text{gap}} = \nu\varepsilon_{\max} t_f \tag{2}$$

where the steel core thickness $t_f = 12.7$ mm (1/2 in.). Poisson's ratio ν equal to 0.5 was used for the steel core because it is subjected to high strains within the plastic region (Wu et al. 2014). The maximum tensile steel strain during the test, $\varepsilon_{\max}$, was assumed equal to 4.0% for design. The wavelength of the buckled steel core l_w in Fig. 9(b) was assumed to be 11 times the thickness of the steel core (Wu et al. 2014) or 140 mm (5.5 in.). The estimated maximum compression force developed by the T-BRB, $P_{\max}$, was estimated as 1.6 times the yield strength of the steel core to account for steel hardening and friction effects between the MPP, hardwood spacer, and steel core; a value of 445 kN (100 kip) was used for $P_{\max}$. Equilibrium of the free-body diagram in Fig. 9(c) results in the value of the force in the bolt, P_b, as

$$P_b = \frac{4P_{\max}\nu\varepsilon_{\max}t_f}{l_w} \tag{3}$$

Eq. (3) results in a bolt force equal to 3.2 kN (727 lb), which was rounded to 4.5 kN (1,000 lb) for design. This force was exerted by the steel core throughout the yielding length for a total of 36 times due to the 140-mm (5.5-in.) wavelength spacing; this results in a total outward force on the casing of 160 kN (36 kip). By allocating 6.7 kN (1.5 kip) of allowable force per bolt, which considers bolt prestressing strength loss during the pneumatic torque tightening process, 24 bolts of 12.7-mm (1/2-in.) diameter were required. The 178-mm (7-in.) bolt spacing provides a total of 28 bolts in the 2.49-m (98-in.) yielding zone. This spacing is conservative and failure involving bolt fracture is precluded so that more important failure modes could be studied.

Full-Scale T-BRB Experiments

Full-scale cyclic experiments were carried out on timber BRBs to verify their performance under cyclic loads for both fatigue and high-strain loading conditions. Composite steel/concrete BRBs are qualified through testing because there are no available methods in existing building codes for their design. T-BRBs were tested according to AISC 341 criteria used for conventional composite steel/concrete BRBs.

T-BRB Loading Protocols, Performance, and Adjustment Factors

The test setup and a typical T-BRB before testing are presented in Fig. 10(a), which shows the bolt pattern. Two loading protocols were used in the experiments: (1) fatigue based, and (2) strain based. Fig. 10(b) shows the fatigue loading protocol for Specimens 1–3; Fig. 10(c) shows the strain loading protocol for Specimens 4–6. The fatigue loading protocol was developed using AISC-341 (AISC 2016) Chapter F4 and Appendix K3. The loading rate used was 46 mm/min (1.8 in./min). Cyclic drift was increased by 0.5% until a 2% drift ratio was reached; subsequently the drift ratio was reduced to 1.5%, which was cycled repeatedly until failure. In the strain loading protocol, cyclic displacement was increased by 0.5% until failure using these drift ratios: 0.5%, 1.0%, 1.5%, 2.0%, 2.5%, 3.0%, and so on until failure. The 2.49-m (98-in.) yield zone length was used to calculate strain. The AISC 341 qualification requires the brace to be tested to two times the design story drift and to achieve a cumulative inelastic deformation (CID) of 200 times the yield deformation.

To define these protocols, the design story drift, Δ_{bm}, and brace yield deformation, Δ_{by}, were determined. The value of Δ_{bm} was calculated at 1.0% story drift, which is 32.5 mm (1.28 in.). The value of Δ_{by} was calculated as follows:

$$\Delta_{b-ysc} = \frac{F_{\text{ysc}}L_{\text{ysc}}}{E} \tag{4}$$

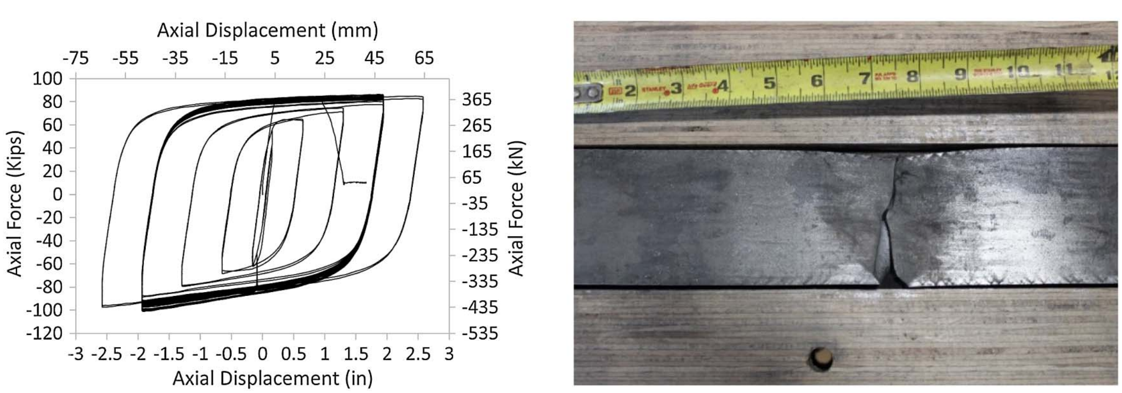

Fig. 11. Specimen 1 hysteresis for fatigue loading protocol and failure mode.

$$\Delta_{b-\text{end}} = 2\frac{A_{sc}}{A_{\text{end}}}\left(\frac{F_{ysc}L_{\text{end}}}{E}\right) \tag{5}$$

$$\Delta_{by} = \Delta_{b-ysc} + \Delta_{b-\text{end}} + \Delta_{\text{apparatus}} \tag{6}$$

The value of $\Delta_{\text{apparatus}}$ was taken as zero because of the instrumentation details; F_{ysc} is the steel yield strength; L_{ysc} is the length of the yield zone; A_{sc} is the area of the yield zone; A_{end} is the area of the end of the BRB core, which includes the stiffeners and cheek plates; and L_{end} is the length of the ends of the core excluding the yield zone. The brace yield deformation Δ_{by} was determined as 4.1 mm (0.16 in.).

The CID of the T-BRB was calculated per AISC 341 (AISC 2016) Table C-K3.1. CID is the accumulation of deformation, both positive and negative, beyond yield, which is converted to multiples of brace yield deformation, Δ_{by}. The T-BRB adjustment factors were determined from data obtained from the hysteresis curves shown in Figs. 11–16. The compression adjustment factor, β, was determined from

$$\beta = \frac{P_{\max}}{T_{\max}} \tag{7}$$

which is the ratio of the maximum measured compressive load to maximum measured tensile load per loading cycle; this ratio must remain below 1.5 per AISC 341 (AISC 2016) to reduce the demand on brace connections and adjoining members. The strain hardening adjustment factor, ω, was determined from

$$\omega = \frac{T_{\max}}{R_y P_{ysc}} \tag{8}$$

as the ratio of maximum measured tensile load to yield force per cycle. Because coupon tests were used to determine yield stress, R_y was taken equal to 1.0; P_{ysc} is the actual yield strength of the steel core. The resulting strain hardening adjustment factor, ω, must be greater than 1.0 according to AISC 341 (AISC 2016).

The adjusted brace strength in compression is given in Eq. (9) and the adjusted strength in tension by Eq. (10)

$$P_{\max} = \beta\omega R_y P_{ysc} \tag{9}$$

$$T_{\max} = \omega R_y P_{ysc} \tag{10}$$

The adjustment factors are used in cyclic tests for conventional composite steel/concrete BRB qualification. Brace connections and adjoining members are designed to resist forces calculated based on the adjusted brace strength in compression and tension.

Results of T-BRB Cyclic Tests

A summary of the T-BRB cyclic test results is presented in Table 3. Hysteresis curves for the six specimens are provided in Figs. 11–16. All hysteresis curves remained stable throughout the tests and the observed failure modes are acceptable based on AISC 341 (AISC 2016) criteria. The CID achieved for the specimens tested using the fatigue load protocol ranged from 5.5 to 7.9 times that required by AISC 341. Specimen 1 failed in tension after 39 cycles as shown in Fig. 11; the steel core in this test fractured

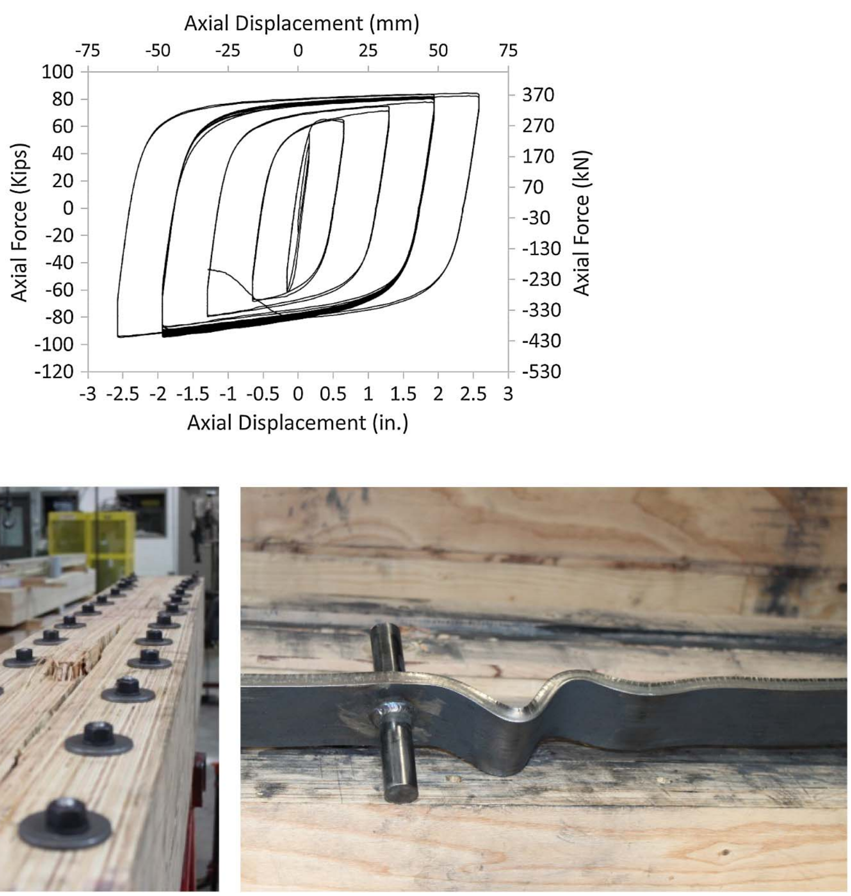

Fig. 12. Specimen 2 hysteresis for fatigue loading protocol and failure mode.

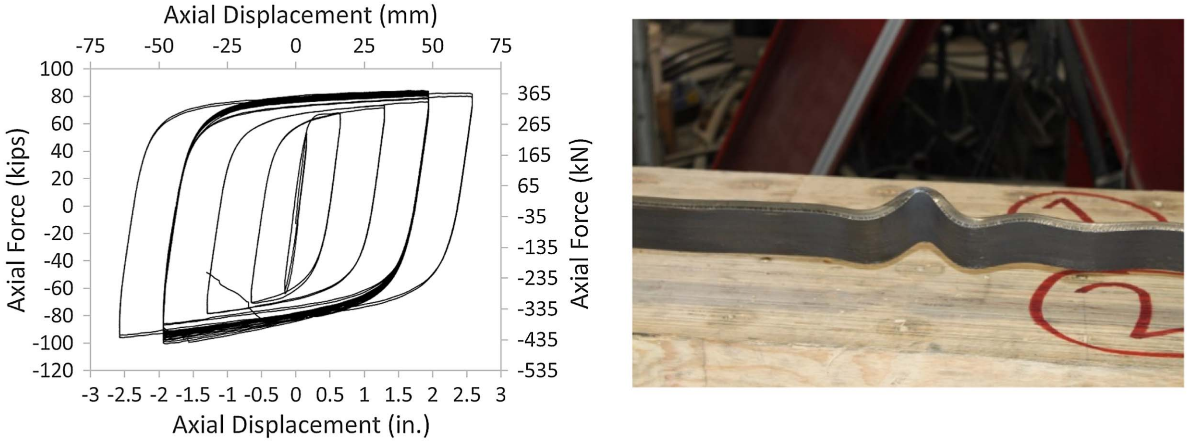

Fig. 13. Specimen 3 hysteresis for fatigue loading protocol and failure mode.

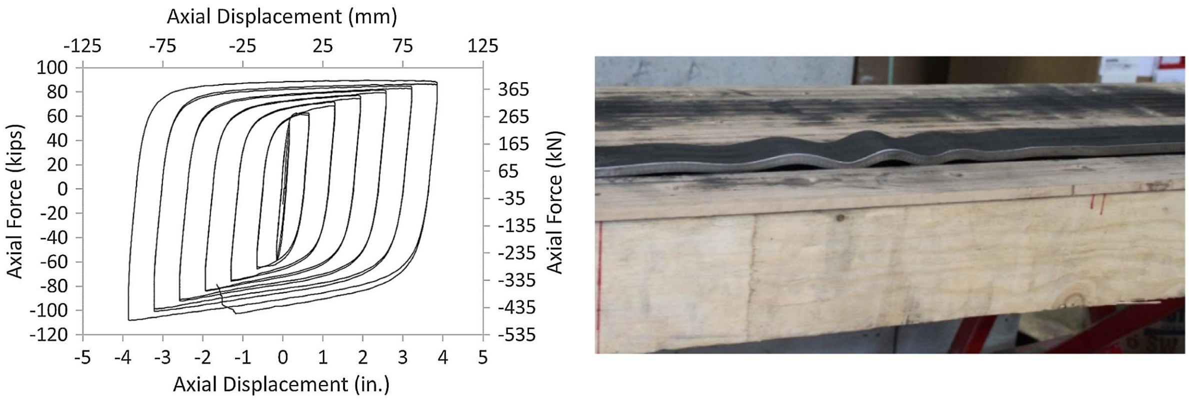

Fig. 14. Specimen 4 hysteresis for strain loading protocol and failure mode.

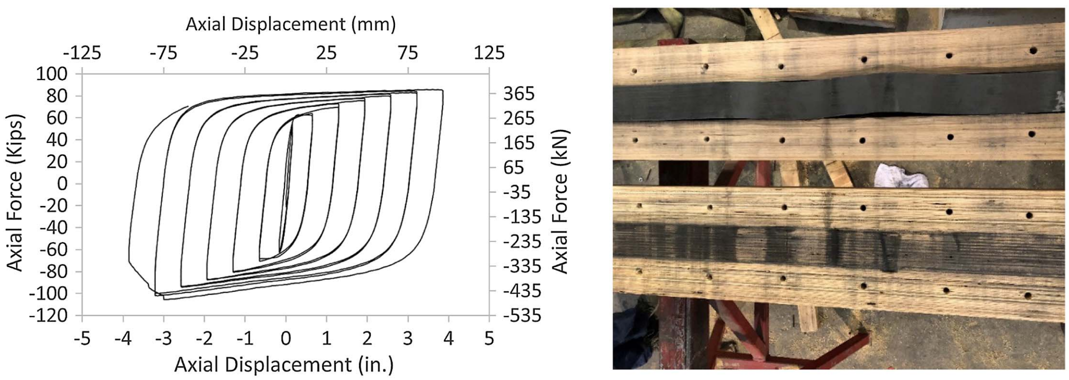

Fig. 15. Specimen 5 hysteresis for strain loading protocol and failure mode.

due to low cycle fatigue, β ranged from 1.05 to 1.20, and ω ranged from 1.00 to 1.40. Specimen 2 failed in compression after 35 cycles as shown in Fig. 12; the MPP layers ruptured from the compressive demand transferred from the steel core, which buckled about the weak axis, β ranged from 1.05 to 1.15, and ω ranged from 1.00 to 1.32. Specimen 3 failed in compression after 28 cycles as shown in Fig. 13; failure was similar to Specimen 2 because the MPP layers ruptured due to demand from weak-axis buckling of the steel core; β ranged from 1.03 to 1.20, and ω ranged from 1.00 to 1.35.

The CID achieved for the specimens tested using the strain load protocol ranged from 2.4 to 2.9 times that required by AISC 341. Specimen 4 failed in compression on the 13th cycle at 3.92% strain, as shown in Fig. 14, which is a significant strain capacity; weak-axis buckling was the dominant failure mode due to casing rupture; β ranged from 1.04 to 1.23, and ω ranged from 1.00 to 1.43. Specimen 5 failed in compression on the 12th cycle at 3.9% strain as shown in Fig. 15; both weak-axis and strong-axis buckling of the steel core were present and the failure mode was a ruptured

J. Struct. Eng., 2021, 147(5): 04021050

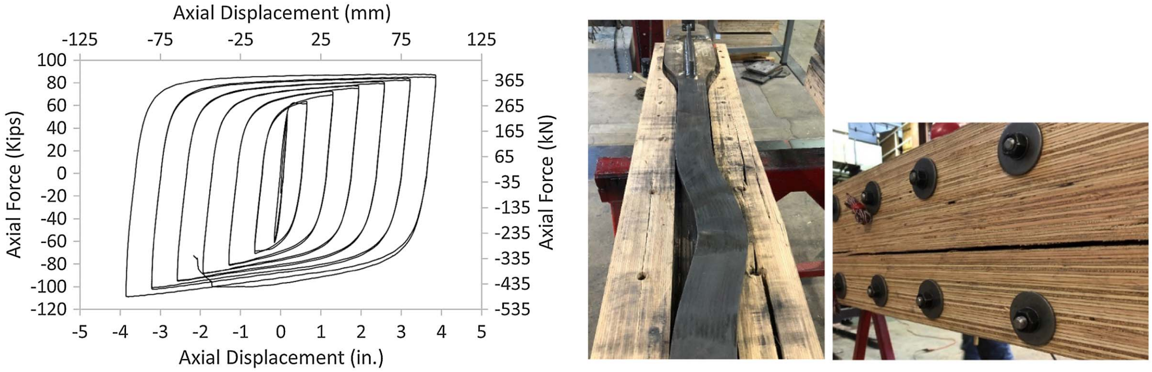

Fig. 16. Specimen 6 hysteresis for strain loading protocol and failure mode.

Table 3. Results for T-BRB tests

Protocol type	Specimen	MPP layout	Max. strain (%)	Max. drift (%)	Cycles to failure	CID	Total hysteretic energy dissipation [kN-m (kip-in.)]
Fatigue	1	60/40	2.61	2.0	39.0	1,571	2,194 (19,422)
	2	80/20	2.61	2.0	35.5	1,416	1,903 (16,840)
	3	100/0	2.61	2.0	28.5	1,107	1,487 (13,161)
Drift	4	100/0	3.92	3.0	13.5	580	807 (7,140)
	5	80/20	3.92	3.0	12.5	488	721 (6,379)
	6	60/40	3.92	3.0	13.5	580	812 (7,188)

and split casing; β ranged from 1.10 to 1.20, and ω ranged from 1.00 to 1.38. Specimen 6 failed on the 13th cycle at 3.9% strain as shown in Fig. 16; strong-axis buckling of the steel core was dominant and the casing layers split and opened due to the strong- axis buckling force; β ranged from 1.11 to 1.25, and ω ranged from 1.00 to 1.41.

Bolt strain was recorded both prior to and during the experiment for two bolts located at the center of the T-BRB. Fig. 17 shows the bolt strain for Specimen 5. Strain increased sharply when the bolts were tightened prior to testing. The bolt strain remained relatively constant during the cyclic test with a slight decrease due to slack being created by permanent timber deformations. A cyclic variation in bolt strain had developed that matched the loading and unloading of the T-BRB, which transferred load to the bolts. Once the casing fractured and split, the bolt strain increased before the experiment was terminated. The highest strain observed during the test was 2,200 microstrain, which is lower than the yield strain, and none of the bolts yielded.

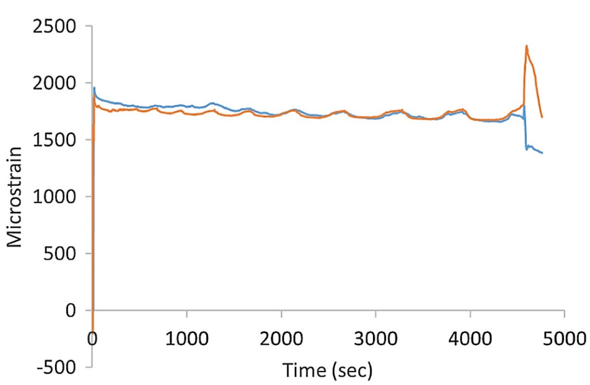

Fig. 17. Specimen 5 bolt strain history for two bolts.

Weak-axis versus strong-axis buckling within the T-BRB is illustrated in Fig. 18. The weak-axis high-mode buckling wavelength, l_w, was measured and recorded after each test. Table 4 lists the average weak-axis wavelength for each specimen. The average weak-axis wavelength was 10 times the core plate thickness, t_c; this is consistent with estimates of the buckling wavelength of conventional BRBs as equal to $11t_c$ (Wu et al. 2014). Strong-axis buckling wavelength was recorded for Specimens 4, 5, and 6, which exhibited this type of deformation; this measurement was difficult to record because the steel cores did not often exhibit a consistent strong-axis buckling throughout the whole length of the yield zone. The average strong-axis buckling wavelength was 483 mm (19 in.), which was 6.33 times the core plate width, w_c; this result is also consistent with the strong-axis buckling wavelength of conventional BRBs, which is approximately equal to $6w_c$ (Wu et al. 2014).

Conclusions

Timber BRBs can be constructed and implemented by combining a steel core with an engineered timber casing. The mechanism for buckling restraint of T-BRBs is new in that the timber casing allows Poisson's expansion of the steel core without an air gap. T-BRBs have advantages compared to composite steel/concrete BRBs that include recyclability, light weight, sustainability, and superior cyclic performance.

The main objective of this research was to design a T-BRB and validate its seismic performance using large-scale cyclic tests. The design of the T-BRB casing was successful and achieved the right balance between strength and stiffness. MPP loaded in the $X-$direction per ASTM D5456 produced a material with very good bearing compression strength. Three MPP materials with layups classified as 60/40, 80/20, and 100/0, which pertain to

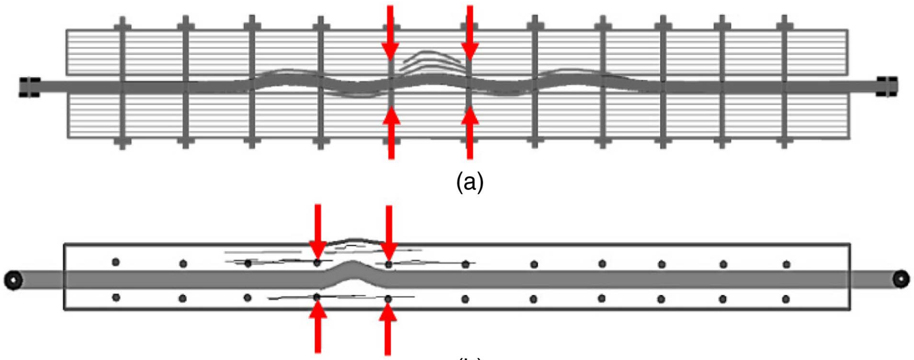

Fig. 18. (a) Weak-axis versus (b) strong-axis steel core buckling.

Table 4. Average weak-axis high-mode buckling wavelength

Specimen	Average wavelength [mm (in.)]
1	140 (5.5)
2	135 (5.3)
3	114 (4.5)
4	135 (5.3)
5	114 (4.5)
6	119 (4.7)

the percentage of 11,031 MPa (1.6×103 ksi) to 6,895 MPa (1.0×103 ksi) laminations were used to build the six T-BRB specimens.

Post-test observations demonstrate that the timber casing, which was designed for 1.5 times the steel core yield load, performed very well. In the majority of the tests, the timber casing was undamaged, which indicates that T-BRBs can be disassembled and inspected after an earthquake to determine whether the steel core should be replaced. A cyclic variation in bolt stress was observed that followed the cyclic loading of the T-BRB; the bolt design was conservative and none of the bolts yielded.

Weak-axis high-mode buckling of the steel core was observed. The average weak-axis buckling wavelength was measured as 10 times the steel core plate thickness, which is consistent with the weak-axis buckling wavelength of composite steel/concrete BRBs. The average strong-axis buckling wavelength was measured as six times the steel core plate width, which is consistent with the strong-axis buckling wavelength of composite steel/concrete BRBs.

The six T-BRBs designed, constructed, and tested in this research exceeded the minimum requirements for uniaxial cyclic tests according to AISC 341. The hysteresis curves were stable and showed that excellent hysteretic energy dissipation was achievable. Each T-BRB achieved a displacement corresponding to two times the design story drift. The T-BRBs reached a cumulative inelastic deformation from 2.4 to 2.9 times the AISC 341 requirement of a cumulative inelastic axial ductility capacity of 200 times the yield displacement.

The T-BRB hysteretic curves showed excellent performance and reached a 3.9% ultimate strain; this is a significant strain and the performance is superior compared to composite steel/concrete BRBs. Using a fatigue loading protocol, the T-BRBs withstood 26.5 to 37.0 cycles at 1.5% strain after being subjected to two cycles at 2.0% maximum strain. The compression adjustment factor, which is important for reducing the demand on brace connections and adjoining members, ranged between 1.05 and 1.25, which is significantly lower than 1.50, the maximum value allowed by AISC 341.

The T-BRB developed in this research is new and innovative and can be used for building a BRBF as a lateral force–resisting system for mass timber buildings in high seismic regions. Suggested areas of additional research include cyclic and shake table tests of mass timber-braced frames utilizing T-BRBs as ductile fuse elements, and the development of analytical models of such systems for seismic design.

Data Availability Statement

The data that support the findings of this study are available from the corresponding author upon reasonable request.

Acknowledgments

The authors would like to thank the US Endowment for Forestry and Communities for its financial support. In addition, the authors want to thank the Forest Products Laboratory for its support and donation of time and materials. The authors want to also thank Vanessa McEntee, Mark Bryant, Bhaskar Kunwar, Duc Tran, Anurag Upadhyay, and Ryan Barton for their assistance. The authors appreciate the comments of the reviewers.

Notation

The following symbols are used in this paper:

A_{end} = area of the ends of the core excluded by the yield zone;
A_{sc} = area of the steel core yielding element;
E = modulus of elasticity;
F_{ysc} = yield strength of steel;
L_{end} = length of the ends of the core excluded by the yield zone;
l_w = wavelength of the buckled steel core;
L_{ysc} = length of the yield zone;
P_b = buckling forces of the steel core in the T-BRB;
$P_{\max}$ = maximum compressive force developed by the T-BRB;
P_{ysc} = actual yield strength of the steel core;
R_y = ratio of the expected yield stress to the specified minimum yield stress;

t_f = original steel core thickness;
$T_{\max}$ = maximum tensile force developed by the T-BRB;
β = compressive adjustment factor;
$\Delta_{\text{apparatus}}$ = displacement of testing apparatus;
$\Delta_{b\text{-end}}$ = deformation at first yield of the steel core element along the nonyielding core length;
Δ_{bm} = design story drift;
Δ_{by} = brace yield deformation;
$\Delta_{b\text{-}ysc}$ = deformation at first yield of the steel core element along the yielding core length;
Δ_{gap} = gap between steel core and MPP casing in T-BRB;
$\varepsilon_{\max}$ = maximum tensile steel strain;
ν = Poisson's ratio; and
ω = strain hardening adjustment factor.

References

Abrahamsen, R. 2017. "Mjøstårnet: Construction of an 81 m tall timber building." In *Proc., Int. Holzbau-Forum IHF 2017*. Bern, Switzerland: Forum Holzbau.

AISC. 2016. *Seismic provisions for structural steel buildings*. AISC 341. Chicago: AISC.

APA (Engineered Wood Association). 2020. *Freres mass plywood panel*. PR-L325. Tacoma, WA: APA.

ASTM. 2011. *Standard test methods for cyclic (reversed) load test for shear resistance of vertical elements of the lateral force resisting systems for buildings*. ASTM E2126. West Conshohocken, PA: ASTM.

ASTM. 2019a. *Standard specification for carbon structural steel*. ASTM A36/A36M-19. West Conshohocken, PA: ASTM.

ASTM. 2019b. *Standard specification for evaluation of structural composite lumber products*. ASTM D5456. West Conshohocken, PA: ASTM.

Black, C. J., N. Makris, and I. D. Aiken. 2004. "Component testing, seismic evaluation and characterization of buckling-restrained braces." *J. Struct. Eng.* 130 (6): 880–894. https://doi.org/10.1061/(ASCE)0733-9445(2004)130:6(880).

Blomgren, H.-E., J. Koppitz, A. Valdes, and E. Ko. 2016. "The heavy timber buckling-restrained braced frame as a solution for commercial buildings in regions of high seismicity." In *Proc., World Conf. on Timber Engineering, Institute for Mechanics of Materials and Structures*. Vienna, Austria: Vienna Univ. of Technology.

CSA (Canadian Standards Association). 2016. *Structural glued-laminated timber.* CSA O122-16 (R2016). Mississauga, ON, Canada: CSA.

Cuadrado, J., M. Zubizarreta, B. Pelaz, and I. Marcos. 2015. "Methodology to assess the environmental sustainability of timber structures." *Constr. Build. Mater.* 86 (Jul): 149–158. https://doi.org/10.1016/j.conbuildmat.2015.03.109.

Genna, F., and P. Gelfi. 2012. "Analysis of the lateral thrust in bolted steel buckling-restrained braces. II: Engineering analytical estimates." *J. Struct. Eng.* 138 (10): 1244–1254. https://doi.org/10.1061/(ASCE)ST.1943-541X.0000564.

Lin, P.-C., et al. 2011. "Seismic design and hybrid tests of a full-scale three-story buckling-restrained braced frame using welded end connections and thin profile." *Earthquake Eng. Str. Dyn.* 41 (5): 1001–1020. https://doi.org/10.1002/eqe.1171.

Murphy, C., C. P. Pantelides, H.-E. Blomgren, and D. R. Rammer. 2019. "Development of timber buckling-restrained braces for mass timber braced frames." In *Proc., INTER Meeting 52*. Karlsruhe, Germany: Karlsruhe Institute of Technology.

Murphy, C. F. 2020. "Development of timber buckling-restrained braces for mass timber braced frames." M.Sc. thesis, Dept. of Civil and Environmental Engineering, Univ. of Utah.

Popovski, M. 2000. "Seismic performance of braced timber frames." Ph.D. dissertation, Dept. of Civil Engineering, Univ. of British Columbia.

Rammer, D. R., and J. J. Zahn. 1997. "Determination of Ylinen's parameter for parallel-strand lumber." *J. Struct. Eng.* 123 (10): 1409–1414. https://doi.org/10.1061/(ASCE)0733-9445(1997)123:10(1409).

Tabatabaei, S. A. R., S. R. Mirghaderi, and A. Hosseini. 2014. "Experimental and numerical developing of reduced length buckling-restrained braces." *Eng. Struct.* 77 (Oct): 143–160. https://doi.org/10.1016/j.engstruct.2014.07.034.

Watanabe, A., Y. Hitomoi, E. Saeki, A. Wada, and M. Fujimoto. 1988. "Properties of brace encased in buckling-restraining concrete and steel tube." In *Proc., 9th World Conf. on Earthquake Engineering*, 719–724. Tokyo: International Association for Earthquake Engineering.

Wu, A.-C., P.-C. Lin, and K.-C. Tsai. 2014. "High-mode buckling responses of buckling-restrained brace core plates." *Earthquake Eng. Struct. Dyn.* 43 (3): 375–393. https://doi.org/10.1002/eqe.2349.

Xu, W., and C. P. Pantelides. 2017. "Strong-axis and weak-axis buckling and local bulging of buckling-restrained braces with prismatic core plates." *Eng. Struct.* 153 (Dec): 279–289. https://doi.org/10.1016/j.engstruct.2017.10.017.

Zahn, J. J., and D. R. Rammer. 1995. "Design of glued laminated timber columns." *J. Struct. Eng.* 121 (12): 1789–1794. https://doi.org/10.1061/(ASCE)0733-9445(1995)121:12(1789).

Zhang, F., X. Chen, L. Chen, Y. Leng, M. Wang, and Q. Xu. 2018. "Shaking table test study on a five story post and beam glulam structuree." In *Proc., World Conf. on Timber Engineering*. Seoul: National Institute of Forest Science.